Advanced Materials Interfaces

ADVANCED MATERIALS INTERFACES Open Access
www.advmatinterfaces.de

RESEARCH ARTICLE OPEN ACCESS

Light-Induced Precipitation of an Inorganic Phosphate for Direct Writing of Thin Films and Templating Complex Mineral Morphologies

Patricia Besirske[1] | Sara Bäum[1] | Helmut Cölfen[1] | Cristina Ruiz-Agudo[1] | Marius Schoettle[2] | Willem L. Noorduin[2,3]

[1]Universität Konstanz, Konstanz, Germany | [2]AMOLF, Amsterdam, The Netherlands | [3]Van't Hoff Institute for Molecular Sciences, University of Amsterdam, Amsterdam, The Netherlands

Correspondence: Cristina Ruiz-Agudo (cristina.ruiz-agudo@uni-konstanz.de) | Marius Schoettle (schoettle@amolf.nl) | Willem L. Noorduin (noorduin@amolf.nl)

Received: 26 August 2025 | **Revised:** 25 November 2025 | **Accepted:** 30 November 2025

Keywords: barium phosphate | continuous mineral thin film | light-induced patterning | photoinduced mineralization | templating

ABSTRACT

Light-induced direct patterning allows intricate spatiotemporal control over microscopic structures and has even been extended to functional inorganic materials. However, while sol–gel-based materials such as silica maintain structural continuity, photoinduced precipitation of salts such as carbonates and phosphates typically suffers from a granular nature and produces loose particle assemblies. In this study, UV-induced release of phosphoric acid from an organic precursor is exploited for locally modulating supersaturation levels. This allows for controlled interplay between photogeneration and precursor supply, for the precipitation of structurally continuous, non-granular barium phosphate from solution. Based on these insights, nanoscopic thin films with controllable thickness are deposited in an illuminated spot. By moving the light beam, this approach is extended to direct writing based on user-defined patterns. Moreover, by triggering photoinduced mineralization within organic templates, complex morphologies can be replicated with high fidelity. This versatility and precision will open new opportunities for the design of functional, biologically relevant inorganic materials.

1 | Introduction

Creating custom shapes and patterns with light-based structuring techniques has become a cornerstone of materials design [1, 2]. For example, advancements in photolithography [3], selective laser sintering [4], and multiphoton polymerization [5–10] now allow the fabrication of intricate polymeric microstructures. These structures can then act as molds for the indirect fabrication of more functional inorganic architectures.

There is also considerable interest in the direct patterning of inorganic matter. Prominent techniques for producing high-performance coatings and thin films include pulsed laser deposition [11, 12] (PLD) or radio frequency sputtering [13–15] (RFS), both widely used for biocompatible materials. With PLD, a laser beam ablates material from a solid target, generating a plume that condenses as a thin film on the substrate. In contrast, RFS uses radio-frequency high-voltage to create a plasma, which then ejects atoms from the target and deposits them onto the desired surface. A continuous layer is typically obtained after subsequent sintering of the deposited material. Sintering can be avoided by techniques such as sol–gel coating [16], in which the precursor material is applied by spin coating to form a thin film that is solidified through drying. These approaches enable the

Advanced Materials Interfaces, 2025; 0:e00771
https://doi.org/10.1002/admi.202500771

fabrication of large, thin film-like structures on flat substrates. There is also a growing interest in creating more intricate spatial patterns, with optical methods offering the most effective route.

The most well-understood example for the direct patterning of inorganic matter with light is silica, which can readily be controlled via light-induced self-assembly [17–21]. Here, UV-activation of a photoacid locally triggers hydrolysis and condensation of a silica precursor in the presence of a templating agent [21]. This spatial control allows precise manufacturing of patterned thin films and 3D shapes [17, 19–21]. Such continuous structures can then provide functionality in advanced filtration and drug-delivery systems [17]. Importantly, for these architectures to be stable and conforming to a nanoscopic template, the produced material must be continuous and monolithic, rather than a granular assembly of particles.

More recently, research has concentrated on light-induced patterning of salts such as inorganic carbonates, sulfates, and phosphates [22]. One strategy exploits the retrograde solubility of these compounds and induces local precipitation via near-infrared light and photothermal heating [23]. Alternatively, UV-induced splitting of precursor molecules has been shown to locally generate phosphate or carbonate anions, thereby causing local supersaturation and leading to nucleation and crystal growth [24, 25]. In contrast to silica, these ionic compounds widen the range of possible applications due to their optical [26–29] and photocatalytic properties [26, 29], as well as biological relevance [30–34]. Subsequent ion exchange of e.g., carbonate salts can even cause conversion into semiconductors for advanced electronic properties [35, 36]. However, these studies focus on light-induced growth of faceted single crystals, nanocomposites, or granular assemblies [37, 38]. Structurally continuous precipitates of pure salts such as phosphates have not been presented, but are a prerequisite for extending into direct writing and additive manufacturing of functional inorganic architectures.

Here, we present a system that allows patterning of an inorganic phosphate with spatiotemporal control and continuous morphology. At the heart of this approach is the photochemically induced splitting of 4-Nitrophenylphosphate (4-NPP) in solution [24]. This UV-light driven process triggers the release of free phosphate ions, which, in the presence of Ba^{2+}-counterions, immediately precipitate as insoluble barium phosphate (Scheme 1). Local irradiation with UV-light provides spatiotemporal control over this precipitation, which can be tracked in situ with a custom-built microscope. Diffusion of unreacted precursor thereby sustains a constantly high supersaturation and ensures the formation of a structurally continuous precipitate inside the user-defined light pattern. This provides spatiotemporal control over barium phosphate deposition, including nanoscopic thin film formation, sub-mm direct writing, and micron-scale templating.

2 | Results

To develop a phosphate precipitation reaction with photochemical control, we investigate how a photolabile molecule can release phosphate ions under UV-irradiation. This prerequisite is met with 4-NPP, a molecule best known for phosphatase activity measurements [39]. Recently, UV-induced splitting of 4-NPP in the presence of calcium ions was shown to cause formation of granular calcium phosphate [24]. Now, we aim for precise spatiotemporal and morphological control over such a precipitation reaction.

It is generally known that the formation of a structurally continuous film via precipitation of an ionic compound is facilitated by: 1) inducing a high initial supersaturation; and 2) maintaining this high supersaturation during the entire precipitation process [40]. By staying in this regime, nucleation dominates over particle growth and nanoscopic clusters aggregate to form a dense and continuous structure [40, 41]. Based on this insight, we target a phosphate salt with a particularly low solubility: barium phosphate. Additionally, we conduct all experiments at an elevated temperature of 60°C, which increases the reaction rate of the 4-NPP splitting reaction. This elevated temperature also synergistically increases the supersaturation due to the retrograde solubility of phosphates [23, 42], thereby creating optimal conditions for UV-induced precipitation of a structurally continuous material.

Barium phosphate is of particular interest due to its high refractive index combined with strong transparency in the ultraviolet range. These optical properties make it an excellent component for advanced optical glasses, particularly those used in laser applications [43]. In addition, barium phosphate serves as a highly adaptable host lattice for dopants such as europium or terbium, enabling precise tuning of emission characteristics and rendering it a versatile platform for engineered luminescent phosphors [44]. Its chemical stability and structural versatility further enhance its appeal, positioning barium phosphate as a promising candidate for photocatalytic applications [26].

We begin this study with an evaluation of the splitting kinetics in aqueous solution via UV–vis spectroscopy (Figure 1a). An initially dominant peak at 312 nm decreases in intensity as the precursor molecule reacts under irradiation. Simultaneously, a peak at 405 nm begins to emerge, attributed to the photoproduct 4-nitrophenolate. A detailed analysis of this time series shows exponential decay of the 4-NPP concentration, consistent with first-order splitting kinetics (Figure 1b) [45]. This behavior entails a time-dependent decrease in the rate of phosphate generation, which is crucial information for understanding how the time-dependent supersaturation will later affect the precipitation reaction, which we aim to control.

In the first precipitation experiment, we bring one side of a glass substrate into contact with a precursor solution of 4-NPP and $BaCl_2$. Irradiation of the entire substrate with UV-light then induces photosplitting and subsequent precipitation of barium phosphate on the substrate surface. Electron microscopy reveals a loose assembly of particles on the substrate, with an average size of 750 ± 230 nm (Figure 1c,d). Elemental mapping proves that these particles consist of barium phosphate, and high-resolution transmission electron microscopy (HRTEM) reveals a nanocrystalline structure (Figure 1e). Besides phosphate, infrared spectroscopy shows a degree of carbonate anions in the material, presumably originating from ambient carbon dioxide (Figure 1f). Overall, these results indicate a system that allows UV-triggered formation of barium phosphate but fails to ensure structural continuity.

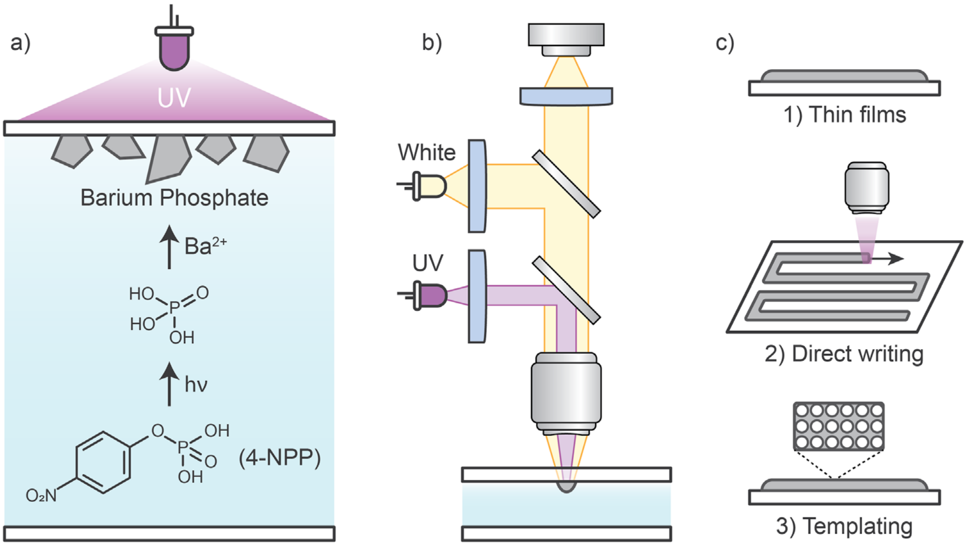

SCHEME 1 | UV-induced phosphate generation and precipitation of barium phosphate. (a) Photochemical reaction of 4-Nitrophenylphosphate (4-NPP) generates phosphoric acid, which precipitates with barium ions to form barium phosphate. (b) The precipitation is followed using a custom-built microscope. (c) Photochemical mineralization process enables thin film formation, direct writing, and templating.

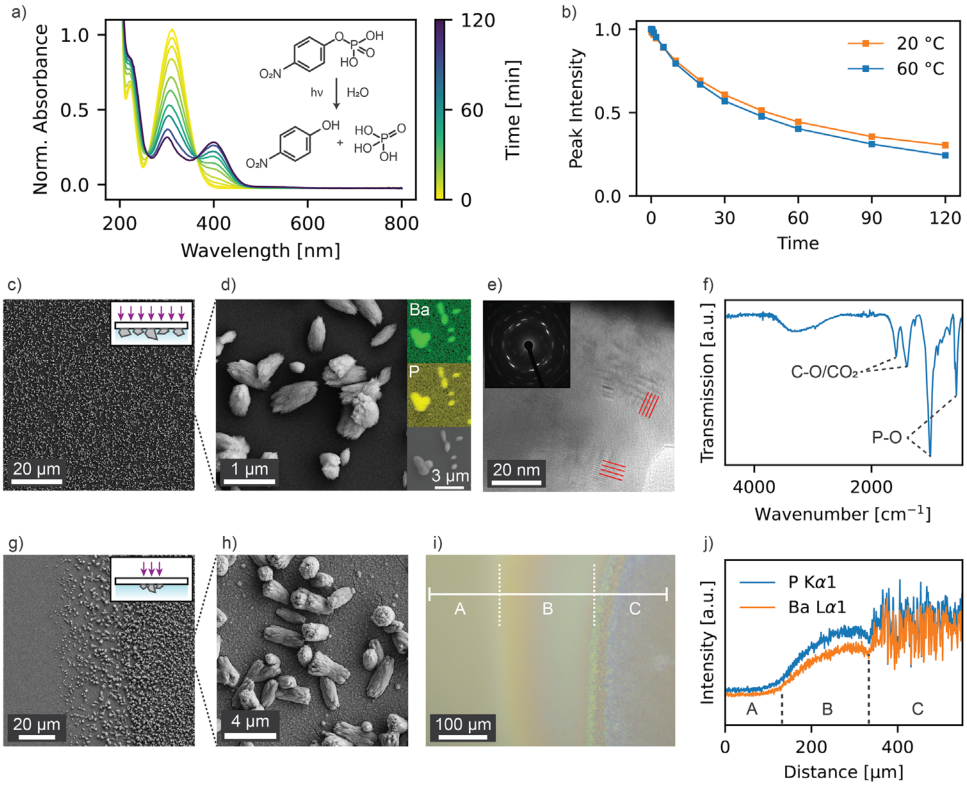

FIGURE 1 | Photoinduced mineralization of barium phosphate. (a) UV–vis spectra measured during the photochemically induced splitting of 4-Nitrophenylphosphate (4-NPP) in an aqueous solution. (b) Decreasing peak intensity at 312 nm indicating the first-order reaction kinetics of 4-NPP for different temperatures. (c) SEM image of particles formed on a glass substrate after irradiation of a solution containing 4-NPP and $BaCl_2$. (d) Higher magnification SEM images and EDX maps showing that these particles consist of barium phosphate. (e) HRTEM image with various orientations of lattice fringes (indicated by red lines) and electron diffraction pattern showing the nanocrystalline nature of the particles. (f) FTIR spectrum indicating the presence of phosphate as well as carbonate from environmental CO_2. (g) SEM image at the edge of an irradiated spot with a diameter of 1 mm. (h) Higher magnification SEM image showing particles that are slightly embedded in a thin film. (i) Light microscopy image at the edge of the spot, showing how at the outer edge of the irradiated area, the precipitation reaction results in a continuous thin film and characteristic interference colors. The inside consists of the previously observed particles and a granular assembly. (j) EDX profiles obtained by scanning from the substrate (A) via the thin film (B) to the granular inner area (C).

We attribute this granular nature and the slightly branched particle morphology to a time-dependent drop in the supersaturation. In accordance with the classic LaMer model [46], a fast increase in the supersaturation causes a burst of nucleation, which in turn initiates a drop in concentration. Since the kinetics study in Figure 1b showed that the precursor molecule 4-NPP is gradually depleted, this suggests that the photogeneration of phosphate ions is insufficient to counteract the decreasing supersaturation. The system therefore remains in the regime of particle growth rather than nucleation. This implies that, in addition to the initially high supersaturation, greater care must be taken to maintain a stable photoactive precursor concentration and ensure a controlled, film-like morphology [40].

To achieve a state where the photoinduced precipitation reaction is constantly supplemented by unreacted 4-NPP, we switch to localized UV-irradiation. The key idea here is to allow diffusion of 4-NPP from the surrounding area to the inside of the irradiated spot and ensure continuous, high supersaturation. Integrating the sample cell in a custom microscope [38] allows us to trigger the reaction exclusively in a UV-irradiated spot with a diameter of 1 mm. After irradiating the sample for 60 min, we analyze the precipitate in this spot, where SEM images again show a particulate, granular morphology (Figure 1g; Figure S1). However, in contrast to global illumination, these particles are now embedded in a film-like component (Figure 1h). Strikingly, optical microscopy at the edge of the irradiated spot shows a colorful ring surrounding the particle-rich center (Figure 1i), consistent with the presence of a thin film producing visible-light interference. This observation is underlined by energy dispersive X-ray spectroscopy (EDX) profiles (Figure 1j) of the barium and phosphorous content, starting on the substrate (A), moving over the thin film (B), and ending in the particle-covered middle section (C). The profiles show a smooth and continuous rise in barium phosphate content when passing over the colorful thin film and become noisy in the irregular and granular inner part of the sample. These results suggest that diffusion of unreacted 4-NPP into the outer part of the irradiated spot locally maintains a high precursor concentration and, in extension, a steady supersaturation. This keeps the system in a state of constant nucleation and results in a continuous thin film morphology [41, 47] in the outer ring with a width of 150 µm.

To fully eliminate unwanted particle growth and exclusively obtain a structurally continuous thin film, we further increase the relative transport into the illuminated area. Therefore, the UV spot size is decreased from 1 mm to 200 µm, which corresponds to a radius smaller than the width of the thin film in Figure 1i. We now conduct in situ light microscopy during the local irradiation and barium phosphate precipitation. Over the course of 60 min, a colorful circular spot emerges in the targeted region (Figure 2a,b; Figure S2). The colors thereby cycle from blue to red, i.e., through the thickness-dependent interference fringes that are expected for nanoscopic thin films consisting of an optically transparent material [48]. This interpretation is corroborated by ex situ height profile measurements of samples where the thin film growth is terminated after different reaction times (Figure 2c). The film thickness of the measured samples ranges from ~150 nm after 30 min, to ~300 nm after 60 min. The growth is approximately linear in time, which stands in accordance with the postulated steady supersaturation and precipitation rate. Furthermore, all profiles are smooth and continuous, highlighting the controlled nature of this growth process.

Ex situ analysis of a sample after 60 min of irradiation confirms the formation of a controlled thin film (Figure 2d). Electron microscopy and elemental mapping show a homogeneous distribution of barium and phosphorous (Figure 2e), consistent with the mechanism of photoinduced phosphate release and precipitation. Furthermore, no topological heterogeneity can be observed, but rather a flat and continuous surface of the thin film. Only a single defect is found in higher magnification images in the form of one nanoscopic crack (Figure 2f). This is a typical failure mode of thin films [49], and most likely results due to mechanical mismatch with the supporting substrate upon full dehydration [50]. Overall, the UV-induced precipitation results in a uniform morphology with precise spatiotemporal control and is also perfectly replicable (Figure S3).

The spatiotemporal control and film-like nature of the precipitate fulfill all prerequisites for direct writing of continuous, extended patterns. Such dynamic control can now easily be achieved by laterally moving the UV-spot along the substrate. To match this movement to the growth rate of the thin film, we set a writing speed of 100 nm/s, which means the spot moves the length of its own diameter in approximately 30 min. The result is a straight line consisting of a barium phosphate thin film with a width of 200 µm, visible as a local color-change in in situ microscopy images (Figure 3a; Figure S4). The interference color of this line matches the color of a circular spot after 30 min of irradiation. This agrees well with the rationale behind the set writing speed and relates to a film thickness of approximately 150 nm. The thickness of the continuous structure can be adjusted by tuning the writing speed, with slower speeds resulting in thicker deposition (Figure S5). Importantly, these properties remain homogeneous along the writing direction, showing no irregularities in the continuous structure. Accordingly, we note these conditions as a first suitable system for light-induced, sub-mm patterning of a phosphate with structural continuity.

Next, we extend the local phosphate growth to 2D patterning and also examine the additive nature of this process. To demonstrate this, a second line is drawn, perpendicular to the initial direction and crossing over the first line (Figure 3b). The result is a homogeneous cross-structure, with the arms and the intersection showing interference colors matching the stationary spot after 30 and 60 min, respectively. This result showcases how the photoinduced precipitation can be extended to arbitrary 2D patterns while maintaining the continuous morphology.

Electron microscopy studies (Figure 3c) also reveal the cross structure, with a clear contrast between substrate, arms, and the intersection. Elemental analysis thereby confirms the presence of barium phosphate. EDX data is also examined as Ba Lα1 profiles across parts of the structure with a single, and a double exposure (Figure 3d). These profiles are smooth, corroborating the same homogeneous morphology as the thin film in Figure 2. Moreover, the profile along the intersection shows a larger amount of deposited material compared to the arms. This additive behavior is further elucidated by detailed elemental composition analysis

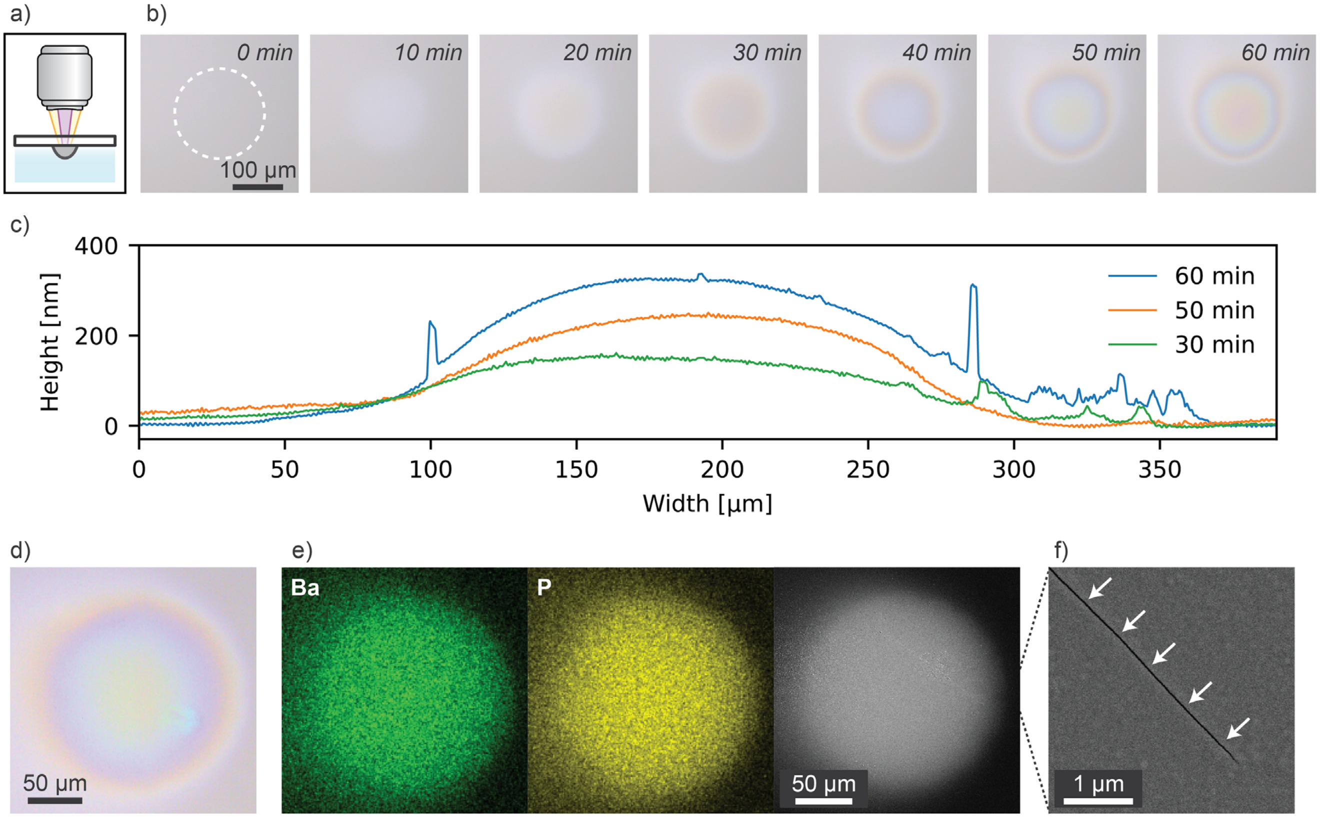

FIGURE 2 | Photoinduced mineralization of barium phosphate thin films. (a) Schematic local irradiation and barium phosphate growth. (b) In situ light microscopy images of a barium phosphate thin film growing in an irradiated spot with a diameter of 200 µm (white circle). The evolving interference fringes and color changes reveal the gradual increase in the film's thickness. (c) Ex situ height profiles of selected spots, measured with a mechanical profilometer. (d) Light microscopy image and (e) EDX maps and SEM image of a spot after 60 min. (f) Higher magnification SEM image showing that the only apparent defect in the film is a single nanoscopic crack (trajectory indicated with arrows).

(Figure 3e). All three elements barium (Ba^{2+}), carbon (from CO_3^{2-}), and phosphorous (from PO_4^{3-}) show a gradual increase from 1) the substrate to 2) the single and 3) the double exposure regions. Overall, these results highlight the possibilities presented by this dynamic yet controlled deposition of barium phosphate in 2D direct writing and, as a future possibility, 3D additive manufacturing of structurally continuous ionic compounds.

Photoinduced precipitation not only enables growth of thin films, but also of more complex morphologies by triggering precipitation in the presence of templates. Growing an inorganic material with a continuous rather than a granular morphology allows it to conform to micro- and nanoscopic geometric confinements of an organic template. The removal of the template leaves behind a continuous morphology that maintains structural integrity, and we exploit this principle here to achieve additional complexity. To complement the 2D writing resolution of a few 100 µm, we aim for a subordinate, periodic pattern on a micron scale. Therefore, we choose a monolayer of 1 µm-sized polystyrene colloids as a template. After local barium phosphate growth around the template and subsequent removal of polystyrene, a porous mesostructure will remain (Figure 4a).

The first step in this process is the assembly of the sacrificial template. Interface mediated self-assembly is applied to produce a uniform, hexagonal monolayer of polystyrene colloids on a glass substrate (Figure 4b) [51, 52]. The colloid size of 1 µm, together with the uniform periodicity results in a diffraction grating with macroscopic structural coloration [53–55]. The coated substrate is then immersed in an aqueous solution of $BaCl_2$ and 4-NPP. Analogous to previous experiments, a circular area with a diameter of 200 µm is irradiated with UV-light for 60 min (Figure 4c; Figure S6). Due to the topography and concomitant light scattering, the evolving barium phosphate structure shows a less pronounced but still recognizable color change in the in situ microscopy data. After the precipitation is complete, the sample is calcined at 500 °C in air to remove the polystyrene colloids and leave behind the templated inorganic component.

After calcination, optical microscopy reveals a circular spot with pronounced structural coloration (Figure 4d). This color is attributed to the high refractive index contrast between barium phosphate and air, and similar diffraction effects as were observed in the original hexagonal template. Electron microscopy substantiates this, showing a periodic mesostructure (Figure 4e,f). Except for some stress-induced cracks, the hexagonal symmetry is homogeneous over the entirety of the deposited spot. Close-up images reveal a morphology of close-packed hollow spheres (Figure 4g; Figure S7). For the most part, gaps in the middle of three adjacent spheres remain unfilled. This indicates overgrowth of the polystyrene colloids during irradiation, with only a slight nanoscale roughness. Overall, the light-induced precipitation of

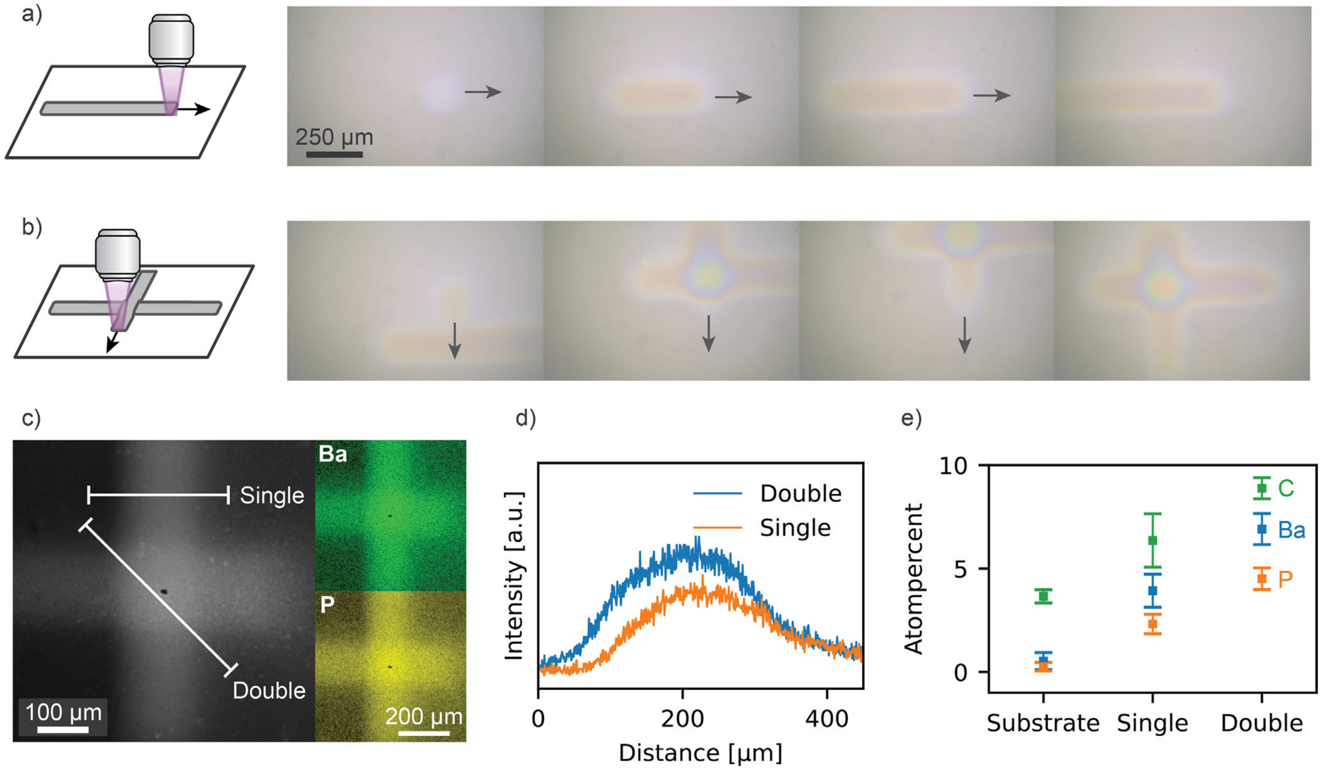

FIGURE 3 | Direct writing of mineralized thin films. (a) Schematic and in situ microscopy images of a barium phosphate thin film line being drawn by horizontally moving the UV-spot at a writing speed of 100 nm/s. (b) Analogous barium phosphate thin film line-growth in the vertical direction, crossing over the first horizontal line. (c) SEM image and EDX maps of the final cross structure. The contrast in the SEM image as well as the barium and phosphate content increases going from the substrate via the single exposed arms toward the double exposed middle of the cross structure. (d) EDX line scan profiles of the Ba Lα1 signal across the vertical line (single) as well as across the intersection of the two lines (double) highlighted in (c). (e) Evaluation of the elemental composition measured by multiple point EDX spectra on the substrate, on the single exposed arms (single), and at the cross' intersection (double).

barium phosphate allows good replication of the sacrificial template and underpins the importance of a continuous morphology for precise patterning procedures.

The spatial control, structural continuity, and patterning freedom make this UV-induced phosphate precipitation a versatile new way of processing ionic compounds. Further research will focus on extending the range of accessible morphologies and allow use-cases that exploit the high optical refractive index of barium salts [28]. Such materials could include sub-micron pores for visible light scattering in passive cooling applications [56], or circular spots with a tailored curvature for microlens fabrication [57]. In contrast to state-of-the-art physical vapor deposition techniques, our method is currently limited to barium phosphate deposition. Future developments will include adjusted formulations and solvent mixtures to tune the solubility of, e.g., calcium and strontium salts, and make these compatible with our system. This could then open a pathway to additive manufacturing of biologically relevant materials. If the method can be extended to calcium phosphate, this would be an ideal starting point for a new addition to direct 3D-printing of artificial bones [58]. Such a process could even be combined with an orthogonal, second precipitation reaction of a different, possibly organic, component, for further structural functionality [59–62]. Finally, the combination of templating and photochemistry could also open a new pathway for the oftentimes challenging research on mineralization in small confinements [63, 64].

3 | Conclusion

In summary, we demonstrate that photoinduced generation of phosphoric acid enables spatiotemporal control over the patterning of an inorganic phosphate salt while maintaining structural continuity. We find that this localization and the continuous morphology rely on an interplay between photochemistry, supersaturation, and diffusion; only if phosphate generation is confined to a small area, can diffusion of unreacted precursor counteract depletion and sustain a constantly high supersaturation. Thereby, the system is kept in a state of nucleation rather than particle growth and a continuous, non-granular structure emerges in the form of a nanoscopic thin film. These findings are corroborated both by a kinetic study of the 4-NPP splitting reaction, as well as precipitation of barium phosphate in illuminated spots of decreasing diameter. Based on this realization we directly write 2D patterns composed of continuous films of barium phosphate. Our precipitation pathway enables the confinement of inorganic material deposition to areas on the order of a few hundred micrometers. This direct local control contrasts with techniques such as PLD and RFS, which typically coat the entire exposed

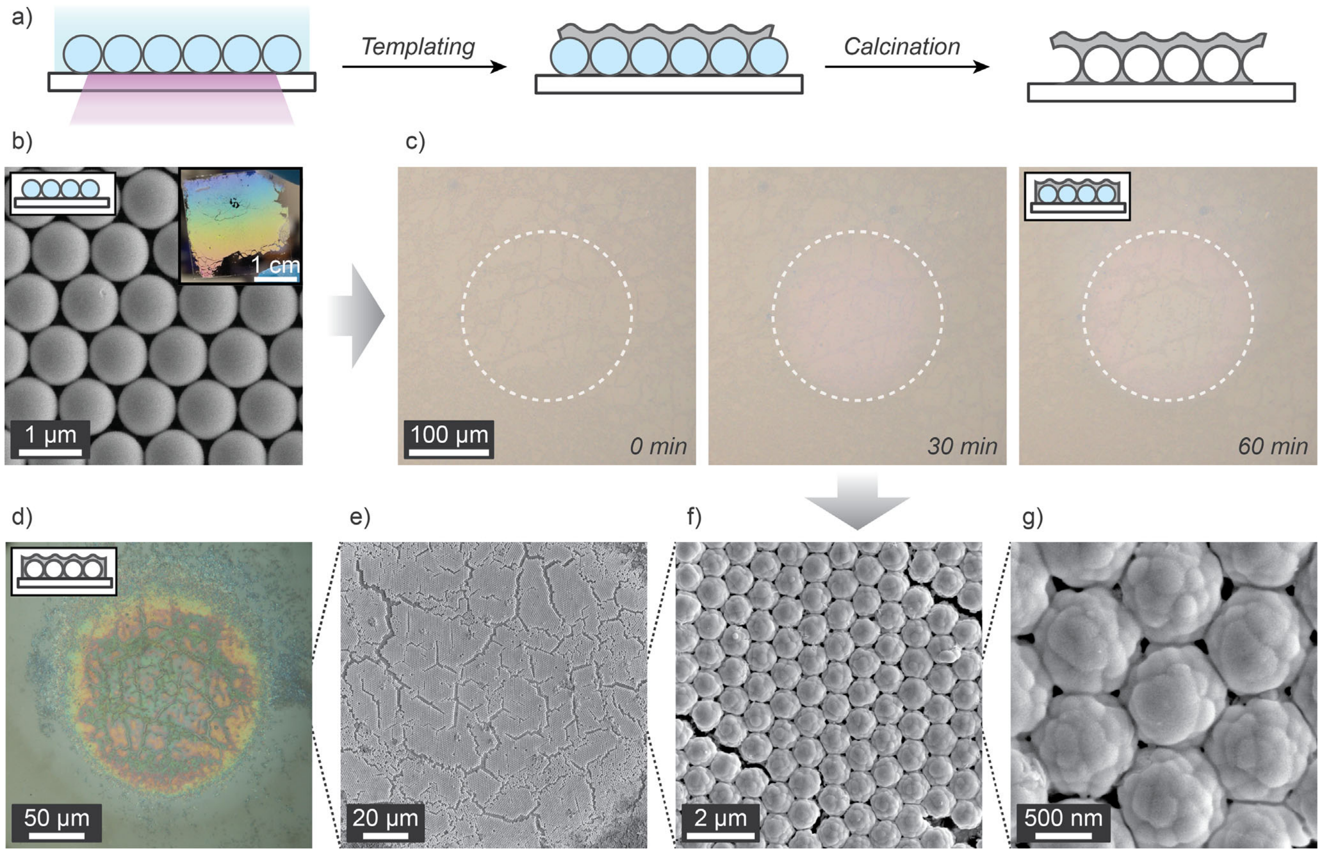

FIGURE 4 | Templated, photoinduced mineralization. (a) A monolayer of polystyrene colloids is immersed in the precursor solution, and UV-irradiation causes overgrowth with barium phosphate. Calcination of the colloids then leaves behind the templated inorganic material. (b) SEM image and photograph of the hexagonal arrangement of polystyrene colloids, which act as a diffraction grating with structural color. (c) In situ microscopy images during UV-irradiation in a circular spot (white circle). (d) Light microscopy image after calcination. (e–g) SEM images of the calcined sample, showing how the barium phosphate replicates the initial colloid array.

substrate. Furthermore, the UV-triggered phosphate generation can proceed in water rather than in high vacuum and at moderate substrate temperatures, making it compatible with a broader range of substrates and environments. Due to its structural continuity, the material can also be controllably precipitated in the confines of a colloidal organic template, which we exploit for the fabrication of a hexagonally ordered mesostructure. These results substantiate the possibility of manufacturing continuous inorganic structures, which could open new pathways in material processing, e.g., for optical elements and micropatterned, high refractive index materials, or, if extended to calcium phosphate, 3D-printing of artificial bones.

4 | Experimental Section/Methods

4.1 | Materials

4-Nitrophenylphosphate (>99%), Barium chloride (>99%), and polystyrene-particles (1 µm, 10 wt.% in water) were obtained from Sigma–Aldrich and used as received. Sodium hydroxide (99.1%) was purchased from VWR.

4.2 | 4-NPP Kinetics

A 1.67 mᴍ 4-NPP solution was prepared by dissolving 0.0124 g of 4-NPP in 20 mL of 0.005 ᴍ NaOH solution. This stock solution was further diluted 1:2 with 0.005 ᴍ NaOH solution and filled into a quartz cuvette. The cuvette was sealed and placed onto an aluminum block to adjust to the temperature prevailing during the irradiation experiment (room temperature or 60°C). The sample was irradiated at 370 nm at full intensity (Kessil PR160L) and measured after distinct time intervals (Kessil PR controller).

4.3 | Global Barium Phosphate Precipitation

A 4-NPP solution was prepared by dissolving 0.0124 g of 4-NPP in 16.6 mL of water. 1 mL of a 0.1 ᴍ NaOH solution was added as well as 2.4 mL of a 0.02 mᴍ barium chloride solution, resulting in a final barium chloride concentration of 2.4 mᴍ and 4-NPP concentration of 1.67 mᴍ. The solution was transferred into the irradiation cassette, which was then sealed. The irradiation cassette was placed on the heating plate and adjusted to the temperature prevailing during the irradiation experiment. Irradiation was applied at full intensity (Kessil PR160L 370 nm lamp with a Kessil PR controller) and after distinct time intervals parts of the cassette were covered. Following the irradiation, the supernatant was removed by flushing the cassette with water. After ejection of the water the cassette was opened, and the front slide was washed with ethanol and blow dried under nitrogen flow.

4.4 | Local Barium Phosphate Precipitation

In a typical experiment, a sample cell was assembled consisting of two clean glass slides separated by a 3 mm thick Viton spacer and filled with the reaction solution. UV-light irradiation of a defined spot on surface then proceeded in a self-built microscope [38]. The light of a 365 nm UV LED (Thorlabs M365L3, 1290 mW output power) was passed through a pinhole of the appropriate size, focused with a plano convex lens (Thorlabs LA4148-UV, $f = 50$ mm), reflected from a dichroic mirror and directed through a 10×/0.30 magnification objective (Nikon Plan Fluor). The temperature was controlled by a bath and circulation thermostat (Huber CC-K6). Motion control was provided by piezo inertia actuators (Thorlabs PIAK10) that had a typical step size of 20 nm. In the imaging part, a cold white light mounted LED (Thorlabs MCWHL5) was collected by an aspheric lens (Thorlabs ACL2520U-DG6-A, $f = 20$ mm). A 10:90 beamsplitter (Thorlabs BSN10R) directed the light through the objective to the sample. The reflected images were collected with the same objective lens and transmitted through the beamsplitter. With help of a tube lens (Thorlabs AC254-200-A-ML), images were recorded by a CMOS camera (Basler Ace acA1920-40gc).

4.5 | Templating

The organic template was prepared by spin-coating the PS-particle suspension at 1000 rpm for 60 s on glass substrates and subsequent interface-mediated assembly via an aqueous solution of SDS (100 mM) and NaOH (1 mM) onto glass substrates [51]. Local barium phosphate precipitation then proceeded identically to the previous experiments on blank glass substrates. After the UV-induced precipitation, washing with water, and drying in air, the particles were removed by calcination in air at 500°C for 2 h, with a heating rate of 10°C/min.

4.6 | Characterization

Fourier-Transform Infrared Spectroscopy (FTIR)-spectra were acquired using a Perkin Elmer 100 Spectrum spectrometer with a Universal Attenuated Total Reflection (UATR) sampling accessory.

UV–vis absorption spectra were measured in a Varian Cary 50 UV–vis Spectrophotometer, with the spectra being measured from 200 to 800 nm in a quartz cuvette (10 mm or 1 mm).

Scanning Electron Microscopy (SEM) analyses were conducted using a Zeiss Gemini 500 with an Oxford Ultim Max 100 detector. The samples were prepared on carbon tape, with some undergoing no additional sputtering and other samples receiving an ITO-coating of 8 nm.

High-resolution transmission electron microscopy (HRTEM) micrographs were measured at a Jeol JEM 2200FS transmission electron microscope, which was operated at 200 kV.

The pH values were determined by means of a SCHOTT laboratory pH Meter CG 843P at room temperature.

Optical microscopy of dry samples proceeded with a Leica DMLP in epi-illumination.

Acknowledgements

The authors thank Jessica Geppert for the HRTEM measurements. Cristina Ruiz Agudo expresses her gratitude to the Zukunftskolleg (University of Konstanz, Excellence Strategy) for its financial support. This manuscript is dedicated to our late colleague and mentor, Helmut Cölfen, who supervised this project and worked on this manuscript, but unfortunately lost his fight against cancer on 28 November 2023.

Conflicts of Interest

The authors declare no conflicts of interest.

Data Availability Statement

Data available on request from the authors.

References

1. H. Kodama, "Automatic Method for Fabricating a Three-dimensional Plastic Model With Photo-hardening Polymer," *Review of Scientific Instruments* 52 (1981): 1770–1773, https://doi.org/10.1063/1.1136492.

2. J. A. Lewis, J. E. Smay, J. Stuecker, and J. Cesarano, "Direct Ink Writing of Three-Dimensional Ceramic Structures," *Journal of the American Ceramic Society* 89 (2006): 3599–3609, https://doi.org/10.1111/j.1551-2916.2006.01382.x.

3. C. W. Hull, "Apparatus for Production of Three-dimensional Objects by Stereolithography", U S Patent 638905, 1984.

4. J. P. Kruth, X. Wang, T. Laoui, et al., "Lasers and Materials in Selective Laser Sintering", *Assembly Automation* 23 (2003): 357–371.

5. R. Raman and R. Bashir, *Essentials of 3D Biofabrication and Translation*, eds. A. Atala and J. J. Yoo (Academic Press, 2015), 89–121.

6. R. J. Mondschein, A. Kanitkar, C. B. Williams, S. S. Verbridge, and T. E. Long, "Polymer Structure-property Requirements for Stereolithographic 3D Printing of Soft Tissue Engineering Scaffolds," *Biomaterials* 140 (2017): 170–188, https://doi.org/10.1016/j.biomaterials.2017.06.005.

7. M. Malinauskas, M. Farsari, A. Piskarskas, and S. Juodkazis, "Ultrafast Laser Nanostructuring of Photopolymers: A Decade of Advances," *Physics Reports* 533 (2013): 1–31, https://doi.org/10.1016/j.physrep.2013.07.005.

8. W. Denk, J. H. Strickler, and W. W. Webb, "Two-photon Laser Scanning Fluorescence Microscopy," *Science* 248 (1990): 73–76, https://doi.org/10.1126/science.2321027.

9. L. Li and J. T. Fourkas, "Multiphoton Polymerization", *Materials Today* 10 (2007): 30–37.

10. J. Zhang, S. Liu, K. Kanokkanchana, et al., "Fabrication of 3D Functional Nanocomposites through Post-Doping of Two-Photon Microprinted Nanoporous Architectures", *Small* 21 (2025): 2403405.

11. V. Nelea, H. Pelletier, M. Iliescu, et al., "Calcium Phosphate Thin Film Processing by Pulsed Laser Deposition and in Situ Assisted Ultraviolet Pulsed Laser Deposition," *Journal of Materials Science: Materials in Medicine* 13 (2002): 1167–1173.

12. I. N. Mihailescu, P. Torricelli, A. Bigi, et al., "Calcium Phosphate Thin Films Synthesized by Pulsed Laser Deposition: Physico-chemical Characterization and in Vitro Cell Response," *Applied Surface Science* 248 (2005): 344–348, https://doi.org/10.1016/j.apsusc.2005.03.111.

13. J. G. C. Wolke, J. P. C. M. van der Waerden, K. de Groot, and J. A. Jansen, "Stability of Radiofrequency Magnetron Sputtered Calcium Phosphate Coatings Under Cyclically Loaded Conditions," *Biomaterials* 18 (1997): 483–488, https://doi.org/10.1016/S0142-9612(96)00164-0.

14. K. A. Prosolov, K. S. Popova, O. A. Belyavskaya, et al., "RF Magnetron-sputtered Coatings Deposited From Biphasic Calcium Phosphate Targets for Biomedical Implant Applications," *Bioactive Materials* 2 (2017): 170–176, https://doi.org/10.1016/j.bioactmat.2017.07.003.

15. T. Narushima, K. Ueda, T. Goto, et al., "Preparation of Calcium Phosphate Films by Radiofrequency Magnetron Sputtering," *Materials Transactions* 46 (2005): 2246–2252, https://doi.org/10.2320/matertrans.46.2246.

16. M. Montazerian, F. Baino, E. Fiume, et al., "Glass-ceramics in Dentistry: Fundamentals, Technologies, Experimental Techniques, Applications, and Open Issues," *Progress in Materials Science* 132 (2023): 101023, https://doi.org/10.1016/j.pmatsci.2022.101023.

17. J. Gluns, L. Zhao, D. Spiehl, et al., "3D Printing of Ordered Mesoporous Silica Using Light-Induced Sol-Gel Chemistry," *Advanced Functional Materials* 34 (2024): 2405511, https://doi.org/10.1002/adfm.202405511.

18. H. Imai, *Handbook of Sol-Gel Science and Technology: Processing, Characterization and Applications*, ed. L. Klein, M. Aparicio, and A. Jitianu (Springer International Publishing, 2018), 569–583, https://doi.org/10.1007/978-3-319-32101-1.

19. H. De Paz-Simon, A. Chemtob, C. Croutxé-Barghorn, et al., "Surfactant-directed Synthesis of Mesoporous Films Made Single-step by a Tandem Photosol-gel/Photocalcination Route," *APL Materials* 2 (2014): 113306, https://doi.org/10.1063/1.4897353.

20. H. De Paz-Simon, A. Chemtob, C. Croutxé-Barghorn, et al., "Periodic Mesostructured Silica Films Made Simple Using UV Light," *The Journal of Physical Chemistry C* 118 (2014): 4959–4966, https://doi.org/10.1021/jp410518k.

21. S. Shi, X. Allonas, C. Croutxé-Barghorn, and A. Chemtob, "Activation of the sol–gel process by visible light-emitting diodes (LEDs) for the synthesis of inorganic films," *New Journal of Chemistry* 39 (2015): 5686–5693, https://doi.org/10.1039/C5NJ00559K.

22. D. Mordini, P. Besirske, J. M. García-Ruiz, et al., "Localized Light-Induced Precipitation of Inorganic Materials", *ChemPlusChem* 90 (2025), 202400487.

23. M. H. Bistervels, B. Antalicz, M. Kamp, H. Schoenmaker, and W. L. Noorduin, "Light-driven Nucleation, Growth, and Patterning of Biorelevant Crystals Using Resonant near-infrared Laser Heating," *Nature Communications* 14 (2023): 6350, https://doi.org/10.1038/s41467-023-42126-4.

24. P. Besirske, A. Menichetti, M. Montalti, et al., "Localized Crystallization of Calcium Phosphates by Light-Induced Processes," *Chemistry—A European Journal* 29 (2023): 202302327, https://doi.org/10.1002/chem.202302327.

25. A. Menichetti, A. Mavridi-Printezi, G. Falini, et al., "Local Light-Controlled Generation of Calcium Carbonate and Barium Carbonate Biomorphs via Photochemical Stimulation", *Chemistry* 27 (2021): 12521–12525.

26. Y. Naciri, A. Ahdour, E. Benhsina, et al., "Ba3(PO4)2 Photocatalyst for Efficient Photocatalytic Application," *Global Challenges* 8 (2024): 2300257.

27. L. Obulapathi, S. H. Babu, B. Sreenivasulu, et al., "Synthesis, Structural, Band Gap, and Optical Properties of Ba3(PO4)2 Hierarchical Structural Materials," *Journal of Materials Science: Materials in Electronics* 33 (2022): 15617–15626.

28. E. T. Y. Lee and E. R. M. Taylor, "Optical and Thermal Properties of Binary Calcium Phosphate and Barium Phosphate Glasses," *Optical Materials* 28 (2006): 200–206, https://doi.org/10.1016/j.optmat.2004.12.010.

29. Y. Chen, B. L. Luan, G.-L. Song, Q. Yang, D. M. Kingston, and F. Bensebaa, "An Investigation of New Barium Phosphate Chemical Conversion Coating on AZ31 Magnesium Alloy," *Surface and Coatings Technology* 210 (2012): 156–165, https://doi.org/10.1016/j.surfcoat.2012.09.009.

30. N. C. Köseoğlu, A. Büyükaksoy, A. Y. Oral, et al., "Hydroxyapatite/Bioactive Glass Films Produced by a Sol–Gel Method: In Vitro Behavior," *Advanced Engineering Materials* 11 (2009): B194–B199.

31. S. V. Dorozhkin, "Calcium Orthophosphates (CaPO4): Occurrence and Properties," *Progress in Biomaterials* 5 (2016): 9–70, https://doi.org/10.1007/s40204-015-0045-z.

32. S. V. Dorozhkin and M. Epple, "Biological and Medical Significance of Calcium Phosphates," *Angewandte Chemie International Edition* 41 (2002): 3130–3146, https://doi.org/10.1002/1521-3773(20020902)41:17%3c3130::AID-ANIE3130%3e3.0.CO;2-1.

33. H. El Feki, J. Michel Savariault, A. Ben Salah, and M. Jemal, "Sodium and Carbonate Distribution in Substituted Calcium Hydroxyapatite," *Solid State Sciences* 2, no. 2 (2000): 577–586, https://doi.org/10.1016/S1293-2558(00)01059-1.

34. J. C. Elliott, *Structure and Chemistry of the Apatites and Other Calcium Orthophosphates*, Vol. 18 (Elsevier Science, 1994).

35. L. Helmbrecht, M. H. Futscher, L. A. Muscarella, B. Ehrler, and W. L. Noorduin, "Ion Exchange Lithography: Localized Ion Exchange Reactions for Spatial Patterning of Perovskite Semiconductors and Insulators," *Advanced Materials* 33 (2021): 2005291, https://doi.org/10.1002/adma.202005291.

36. T. Holtus, L. Helmbrecht, H. C. Hendrikse, et al., "Shape-preserving Transformation of Carbonate Minerals Into Lead Halide Perovskite Semiconductors Based on Ion Exchange/Insertion Reactions," *Nature Chemistry* 10 (2018): 740–745, https://doi.org/10.1038/s41557-018-0064-1.

37. M. H. Bistervels, N. T. Hoogendoorn, M. Kamp, H. Schoenmaker, A. M. Brouwer, and W. L. Noorduin, "Light-controlled Morphological Development of Self-organizing Bioinspired Nanocomposites," *Nanoscale* 16 (2024): 2310–2317, https://doi.org/10.1039/D3NR05828J.

38. M. H. Bistervels, M. Kamp, H. Schoenmaker, A. M. Brouwer, and W. L. Noorduin, "Light-Controlled Nucleation and Shaping of Self-Assembling Nanocomposites," *Advanced Materials* 34 (2022): 2107843, https://doi.org/10.1002/adma.202107843.

39. D. F. McCain and Z.-Y. Zhang, *Methods in Enzymology*, ed. R. Iyengar and J. D. Hildebrandt Vol. 345 (Academic Press, 2002): 507–518.

40. A. R. Pascoe, Q. Gu, M. U. Rothmann, et al., "Directing Nucleation and Growth Kinetics in Solution-processed Hybrid Perovskite Thin-films," *Science China Materials* 60 (2017): 617–628, https://doi.org/10.1007/s40843-017-9043-y.

41. F. Chen, W. Jie, and X. Cai, "Effects of Supersaturation on CdS Film Growth From Dilute Solutions on Glass Substrate in Chemical Bath Deposition Process," *Thin Solid Films* 516 (2008): 2823–2828, https://doi.org/10.1016/j.tsf.2007.04.167.

42. H. McDowell, T. M. Gregory, and W. E. Brown, "Solubility of Ca(5)(PO(4))(3)OH in the System Ca(OH)(2)-H(3)PO(4)-H(2)O at 5, 15, 25, and 37°C",*Journal of Research of the National Bureau of Standards Section A, Physics and Chemistry* 81, no. 2 (1977): 273.

43. P. Ramprasad, C. Basavapoornima, C. R. Kesavulu, et al., "Spectroscopic Properties of Er3+-doped Barium Phosphate Glasses for Optical Gain media", *Results in Optics* 12 (2023), 100489.

44. B. I. Lazoryak, Y. Y. Dikhtyar, D. A. Spassky, et al., "Synthesis and Photoluminescence Properties of Ba3 (PO4) 2: Eu3+/2+ Phosphors," *Materials Research Bulletin* 176 (2024): 112799, https://doi.org/10.1016/j.materresbull.2024.112799.

45. K. Holbrook and L. Ouellet, “The Non-enzymatic Hydrolysis of p-nitrophenyl Phosphate,” *Canadian Journal of Chemistry* 36 (1958): 686–690, https://doi.org/10.1139/v58-096.

46. V. K. LaMer and R. H. Dinegar, “Theory, Production and Mechanism of Formation of Monodispersed Hydrosols,” *Journal of the American Chemical Society* 72 (1950): 4847–4854, https://doi.org/10.1021/ja01167a001.

47. M. Kostoglou, N. Andritsos, and A. J. Karabelas, “Incipient CdS Thin Film Formation,” *Journal of Colloid and Interface Science* 263 (2003): 177–189, https://doi.org/10.1016/S0021-9797(03)00133-4.

48. S. Kinoshita and S. Yoshioka, “Structural Colors in Nature: The Role of Regularity and Irregularity in the Structure,” *Chemphyschem* 6 (2005): 1442–1459, https://doi.org/10.1002/cphc.200500007.

49. T. Ye, Z. Suo, and A. G. Evans, “Thin Film Cracking and the Roles of Substrate and Interface,” *International Journal of Solids and Structures* 29 (1992): 2639–2648, https://doi.org/10.1016/0020-7683(92)90227-K.

50. W. P. Lee and A. F. Routh, “Why Do Drying Films Crack?,” *Langmuir* 20 (2004): 9885–9888, https://doi.org/10.1021/la049020v.

51. M. Retsch, Z. Zhou, S. Rivera, et al., “Fabrication of Large-Area, Transferable Colloidal Monolayers Utilizing Self-Assembly at the Air/Water Interface,” *Macromolecular Chemistry and Physics* 210 (2009): 230–241, https://doi.org/10.1002/macp.200800484.

52. N. Vogel, L. de Viguerie, U. Jonas, C. K. Weiss, and K. Landfester, “Wafer-Scale Fabrication of Ordered Binary Colloidal Monolayers With Adjustable Stoichiometries,” *Advanced Functional Materials* 21 (2011): 3064–3073, https://doi.org/10.1002/adfm.201100414.

53. A. L. Ingram and A. R. Parker, “A Review of the Diversity and Evolution of Photonic Structures in Butterflies, Incorporating the Work of John Huxley (The Natural History Museum, London From 1961 to 1990),” *Philosophical Transactions of the Royal Society B: Biological Sciences* 363 (2008): 2465–2480, https://doi.org/10.1098/rstb.2007.2258.

54. M. Kolle, P. M. Salgard-Cunha, M. R. J. Scherer, et al., “Mimicking the Colourful Wing Scale Structure of the Papilio blumei Butterfly,” *Nature Nanotechnology* 5 (2010): 511–515, https://doi.org/10.1038/nnano.2010.101.

55. N. Vogel, S. Utech, G. T. England, et al., “Color From Hierarchy: Diverse Optical Properties of Micron-sized Spherical Colloidal Assemblies,” *Proceedings of the National Academy of Sciences* 112 (2015): 10845–10850, https://doi.org/10.1073/pnas.1506272112.

56. Y. Dong, H. Han, F. Wang, et al., “A Low-cost Sustainable Coating: Improving Passive Daytime Radiative Cooling Performance Using the Spectral Band Complementarity method,” *Renewable Energy* 192 (2022): 606–616.

57. S. Cai, Y. Sun, H. Chu, W. Yang, H. Yu, and L. Liu, “Microlenses Arrays: Fabrication, Materials, and Applications,” *Microscopy Research and Technique* 84 (2021): 2784–2806, https://doi.org/10.1002/jemt.23818.

58. B. Leukers, H. Gülkan, S. H. Irsen, et al., “Hydroxyapatite Scaffolds for Bone Tissue Engineering Made by 3D Printing,” *Journal of Materials Science: Materials in Medicine* 16 (2005): 1121–1124.

59. R. H. M. van der Meijden, D. Daviran, L. Rutten, et al., “A 3D Cell-Free Bone Model Shows Collagen Mineralization is Driven and Controlled by the Matrix,” *Advanced Functional Materials* 33 (2023): 2212339, https://doi.org/10.1002/adfm.202212339.

60. Y. Xu, F. Nudelman, E. D. Eren, et al., “Intermolecular Channels Direct Crystal Orientation in Mineralized Collagen,” *Nature Communications* 11 (2020): 5068, https://doi.org/10.1038/s41467-020-18846-2.

61. L. K. Grunenfelder, N. Suksangpanya, C. Salinas, et al., “Bio-inspired Impact-resistant Composites,” *Acta Biomaterialia* 10 (2014): 3997–4008, https://doi.org/10.1016/j.actbio.2014.03.022.

62. M. J. Olszta, X. Cheng, S. S. Jee, et al., “Bone Structure and Formation: A New Perspective,” *Materials Science and Engineering: R: Reports* 58 (2007): 77–116, https://doi.org/10.1016/j.mser.2007.05.001.

63. F. C. Meldrum and C. O’Shaughnessy, “Crystallization in Confinement,” *Advanced Materials* 32 (2020): 2001068, https://doi.org/10.1002/adma.202001068.

64. E. Loste, R. J. Park, J. Warren, and F. C. Meldrum, “Precipitation of Calcium Carbonate in Confinement,” *Advanced Functional Materials* 14 (2004): 1211–1220, https://doi.org/10.1002/adfm.200400268.

Supporting Information

Additional supporting information can be found online in the Supporting Information section.

Supporting file: admi70353-sup-0001-SuppMat.pdf